Liquid Crystals
Publication details, including instructions for authors and subscription information:
http://www.informaworld.com/smpp/title~content=t713926090

Comparison of the rupture dynamics of smectic bubbles and soap bubbles

Frank Müller[a]; Ralf Stannarius[a]
[a] Otto-von-Guericke Universität Magdeburg, FNW-IEP, Magdeburg, Germany

To cite this Article Müller, Frank and Stannarius, Ralf(2009) 'Comparison of the rupture dynamics of smectic bubbles and soap bubbles', Liquid Crystals, 36: 2, 133 — 145
To link to this Article: DOI: 10.1080/02678290802699300
URL: http://dx.doi.org/10.1080/02678290802699300

Liquid Crystals,
Vol. 36, No. 2, February 2009, 133–145

Taylor & Francis
Taylor & Francis Group

Comparison of the rupture dynamics of smectic bubbles and soap bubbles

Frank Müller* and Ralf Stannarius

Otto-von-Guericke Universität Magdeburg, FNW-IEP, 39106 Magdeburg, Germany

(Received 13 October 2008; final form 17 December 2008)

The rupture of soap films has attracted scientific interest for over a century, but only few qualitative and quantitative experiments of bursting soap bubbles have been reported so far. Thermotropic smectic films behave, in many respects, in a very similar manner to lyotropic (soap) films. We compare the rupture dynamics of smectic A bubbles on a qualitative level with that of soap bubbles. Our attention is focused on the velocity of the progressing rim around the growing hole, the stability of this rim, changes in the thickness of the film during rupture and the propagation of mechanical waves ahead of the rim in the remaining film. Differences in the internal structures of soap films and smectic films manifest themselves in different rupture characteristics. The experiments help us to understand the dynamical properties of quasi-two-dimensional liquid films far from their mechanical equilibrium.

Keywords: rupture dynamics; thin films; smectic liquid crystal; soap

1. Introduction

Certain liquid materials with an internal layered molecular structure are able to form stable free-standing films. A well-known example is soap bubbles, stabilised by surfactant layers at the film surface. In addition to soap solutions, thermotropic liquid crystals represent materials with an inherent molecular layering. In a free-standing smectic film with two liquid–air interfaces, the layers are arranged parallel to the film surfaces, and this order is transferred into the internal of the film, thus stabilising the film against thickness fluctuations, spontaneous hole formation and rupture. This configuration is metastable because of its large surface energy as compared with, for example, a compact droplet of the same liquid volume. When the film is sufficiently disturbed, for example, when a freely suspended film is pierced with a hole in its equilibrium shape, the film is rapidly destroyed. The excess of surface energy is released and partially transformed into kinetic energy of the material in the rim around the opening hole. The final state is reached when the film material is collected in one or multiple small droplets, and in the meniscus if the film or bubble has been supported by a solid frame or capillary.

About a century ago, Athanase Dupré and Lord Rayleigh proposed a model of the film dynamics during the rupture process (*1–3*). The early models started from the assumption that the released surface energy is completely transformed into kinetic energy of the film material. Quantitative corrections concerning the rim velocity were introduced around 1960 by Culick (*4*) and Taylor (*5*). Today, the following model for the burst of a thin liquid film (or bubble) appears to be generally accepted.

(i) When a hole opens in the film, its edge velocity depends on the film thickness δ, the density ρ and the surface tension σ of the material.
(ii) The velocity of the edge (Culick's velocity) is

$$v = \sqrt{2\sigma/\rho\delta}. \quad (1)$$

In this model, there is no initial acceleration phase of the rim.
(iii) The rim separating the hole from the film collects all of the film material during rupture; the film far from the rim stays at rest.
(iv) In the case when the film thickness is constant over the whole film, the hole grows with constant velocity, it expands homogeneously in all lateral directions. The shape of the hole is circular in that case.

This model implies that half of the surface energy contributes to the kinetic energy of the moving rim and the other half of that energy is dissipated. The physical basis for this model is the assumption of the validity of the momentum balance, which relates the capillary forces in the film to the increasing momentum of the rim. It follows that the mechanical energy is not conserved. The influences of the surrounding medium (air) is neglected. Dissipation is the natural consequence of the assumption that the rapidly moving

*Corresponding author. Email: frank.mueller@physik.uni-magdeburg.de

ISSN 0267-8292 print/ISSN 1366-5855 online

DOI: 10.1080/02678290802699300
http://www.informaworld.com

rim permanently hits the film material at rest. This material is then accelerated practically instantly when it is absorbed into the rim. The details of the dissipation processes are not relevant here.

Since this basic model was established, additional phenomena have been discovered which are, in part, incompatible with the model. It has been shown in further studies that one has to develop a more detailed description of the rupture process. The most striking phenomenon during the rupture of soap films, discovered by McEntee, Mysels and Frankel is the appearance of a considerable disturbance in front of the rim, which is called the aureole by these authors (*6, 7*). The authors assume a stepwise thickening $\Delta\delta$ of the film. This step travels with constant velocity away from the rim. For a step velocity higher than the rim velocity, the surface tension of the aureole has to be lower than that of the thinner, undisturbed film.

In the simple model described above, the rim has a cylindrical shape and the hole confined by the rim is perfectly round. In experiments, even in the early snapshot images by Ranz (*8*) or in the bursting soap bubble studies by Pandit and Davidson (*9*), however, it is evident that the rim does not remain compact in general; a lateral instability occurs. The edge of the growing hole frays out during rupture. This results in the formation of droplets released from the rim, and hence the rim contains less material than in the ideal model. This fact has been recognised in soap film experiments. For example, by McEntee and Mysels (*6*), Pandit and Davidson (*9*), Evers *et al.* (*10, 11*) and in our experiments with thin thermotropic smectic films (*12*).

McEntee and Mysels (*6*) have reported a rim velocity much smaller than Culick's prediction for soap films thinner than around 100 nm. In this film thickness range, the velocity decreases strongly with deceasing film thickness. This has been confirmed by Evers *et al.* (*10, 11*), who studied the rupture behaviour of Newton black films. The authors assume that the influence of both the surrounding air and the elastic deformations of fluid elements during the entrance from the resting film into the moving rim have to be taken into account.

We note that both the above-mentioned soap films and smectic films are referred to as inviscid, even though dissipation is involved in the propagation of the rim. In contrast to these low-viscosity systems, Debrégeas *et al.* (*13, 14*) have studied the rupture of bubbles formed by highly viscous liquids. They used polymer melts (polydimethylsiloxane (PDMS)) with high molecular weight, the viscosity η being of the order of kilopascals. Such bubbles show qualitatively different rupture characteristics. The rim accelerates exponentially, until its velocity reaches a limiting value at a radius of about $R_c = \eta\sqrt{2\delta/\rho\sigma}$. The velocity fields in viscous films has been visualised by means of tiny glass particles dispersed on the film surface. The film velocity as a function of the distance r from the expanding hole obeys a relation $v\,(r) \propto 1/r$, that is, the film thickness increases globally during the rupture process.

Comparably few published experiments so far deal with rupture or collapse of thin smectic films. On the other hand, smectic films offer a number of advantages for quantitative studies of the rupture dynamics, compared with soap films. One of their advantages over soap solutions is that the are composed of pure, one-component mesogenic material; other advantages are the absence of drainage problems, the homogeneity of the film thickness and a higher accuracy of film thickness measurements. The viscosity of smectic liquid crystals is often considerably larger than that of water, of the order of 50 mPa for the material studied here (*15*), but it is still orders of magnitude below that of high-molar-mass polymers. Like soap films, their dynamics can be described rather well within the inviscid bubble model and (1) (see (*12*)).

Today, the rapid progress in high-speed video imaging allows us to analyse the rupture processes in thin liquid films in great detail (*16*). In this study, we compare experimentally the rupture of both soap and smectic A bubbles in order to obtain insight into similarities and differences of the film dynamics in both structures, and in order to understand the nature of the anomalies described above. The two types of a system differ in their inherent structure and thus the rupture process in detail has slightly different features. Soap films are typically made of amphiphile surfactants dissolved in water. At certain surfactant concentrations the mixture tends to form bilayers with a variable amount of water in between. There exists an ordered, but not homogeneous layer structure. Usually, in particular in gravitational fields, one finds film thickness gradients across the film. In contrast to soap films, mesogens in a smectic A material arrange in layers of well-defined thickness δ_0 of the order of the molecular length. The orientational order parameter of the mesogens is typically about 0.8. The film consists locally of a number of N stacked identical layers (except for small influences of the surface). After the smectic film has reached equilibrium with its meniscus, both N and the film thickness $\delta = N\,\delta_0$ are constant across the whole film, or at least over large portions of the film surface. Any thickness inhomogeneity in the film implies the formation of dislocations in the smectic layer arrangement and is thus energetically unfavourable. Islands (excess layers) or holes (depletion of layers) vanish in equilibrium.

2. Experimental setup

A schematic of the experimental setup, where the two illumination geometries (setups 1 and 2) have been combined for simplicity, can be seen in Figure 1. A collimated monochromatic light beam (λ = 535 nm) of approximately 2 cm in diameter serves as the light source. This allows the film thickness profile to be determined even during rupture. The rupture process is typically finished within less than 3 ms after initiation. Therefore, we employ an ultrafast camera (*Photron* Ultima APX) mounted on a long-range microscope (*Infinity*, K2). An additional digital camera (*Nikon* Coolpix 4500) is mounted on a second adapter of the microscope to monitor the bubble before rupture.

We compare the behaviour of the liquid crystal 8CB (4′-Octyl-biphenyl-4-carbonitrile) and an commercially available soap solution (*Pustefix*, Dr Rolf Hein GmbH & Co. KG). 8CB has the phase sequence Cr 21.5°C SmA 33.5°C N 41.5°C I. It is in the smectic A phase at the temperature of the measurements, 26°C.

Even before rupture, the differences in the internal structures described above leads to differences in the bubble behaviour. The smectic liquid crystal films are stable: there is no ageing over time periods of several days. We let the bubbles equilibrate, so that the whole film is of uniform thickness δ before puncture. Usually, a period of about 1 hour was sufficient to eliminate islands and holes. In 8CB, the thinnest part of the freshly drawn film spreads slowly over the whole film. In contrast, soap films are not long-time persistent; they suffer from drainage. One finds substantial vertical film thickness gradients (due to gravity), in all soap bubble experiments. A slow downward material flow results in a successive thinning of the top. For the initiation of the rupture of the smectic liquid crystal films we have used a glass needle. The rupture of the soap films in practice did not need to be initiated. The bubbles burst within 2 min following preparation as a consequence of drainage.

The study of hole growth and of the global shapes of the bursting structures is preferably performed in transmitted light. In some experiments, however, we have observed the bubbles under indirect illumination, that is, the light source for transmission optics has been replaced by a diffuse light source illuminating the bubbles perpendicularly to the observation axis. The background was kept dark. The detected signal is a superposition of the light scattered by the liquid plus some localised reflections in the bubble (which can be ignored in the evaluation). This illumination geometry is useful for the analysis of details during rupture, in particular the fragmentation of the hole edge.

The film thickness is determined with an optical method as described in (*17*). For that purpose we have used monochromatic illumination. The accuracy is $\pm$10 nm for smectic A bubbles and $\pm$20 nm for soap bubbles. One of the problems with optical film thickness measurements of soap bubbles is that the transmitted light passes the film at the front and back side of the bubble, and in case of inhomogeneous film thickness, the superposition of the two interference textures is not unambiguous.

3. Experimental results

The basic features of the bubble burst processes have been described previously. In a study of soap bubbles by Pandit and Davidson (*9*), attention was focused on the determination of the rupture velocity, and the authors have verified the momentum conservation model of (1) with satisfactory accuracy. In addition, they have reported a decomposition of the rim into droplets. The average film thickness in these experiments has been determined before rupture from integral current measurements, experimental data on the local film thickness are not available. One should also note that Pandit and Davidson assumed in their experiments that the rim recesses with uniform and constant speed. This is correct when the soap film is

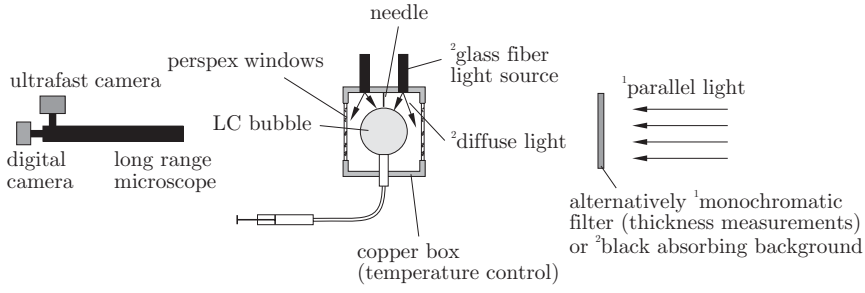

Figure 1. Sketch of the experimental setup. Most of the experiments are performed in the transmission geometry (respective parts are labeled with 1); in some experiments, dark field illumination (labeled 2) has been employed.

uniformly thick everywhere. We analyse this assumption below.

Some of these findings for soap films have also been reproduced in a study of smectic bubbles (*12*). Our earlier measurements confirmed the momentum balance model and the inviscid film dynamics quite well, although a small systematic deviation of the rim velocity from Culick's prediction to lower values has been observed. The velocity determined experimentally amounts to about 80% of the theoretical value of (1). In thin smectic A films, even the instability of the film edge has been reproduced. The rim decomposes into small droplets, whereas in thick films (micrometres and above), the rim remains straight. In contrast to the soap film experiments of Pandit and Davidson, the film thickness of the smectic A bubbles could be measured locally, and data have even been obtained dynamically during the burst. In addition to a slight thickening of the complete film, we have discovered that bursting smectic bubbles with a film thickness in the micrometre range start to scatter light during the rupture process. This feature has not been considered in soap films before. In the following experiments, we compare two features of the rupture process for soap and smectic A bubbles.

(i) We study the light scattering of the film in the transmission geometry during rupture. This scattering is a consequence of the propagation of transversal mechanical waves in the film plane. A possible interpretation is given below.
(ii) We analyse the thickness change of the films during rupture.

3.1 Initial thickness

Before the rupture process starts, we take images of the bubbles in monochromatic light or in white transmitted light to determine the film thickness, either from interference rings or from the interference colours, respectively. The latter approach gives only a rough measure of the thickness range, while the images under monochromatic illumination produce quantitative results. Figure 2 shows the optical appearance of a uniform 1.785 μm thick bubble: the left-hand part shows the experimental image of one hemisphere in 535 nm monochromatic light, the right-hand side gives the calculated image. Since the indices of refraction of 8CB, n_e = 1.673, n_o = 1.524 at 27°C, are known (*18*), the film thickness is the only fit parameter in the model. The numbers and positions of the interference fringes are precise indicators of the film thickness. The model makes the well-founded assumption that the smectic film has the same thickness on the front and back sides of the bubble. The concentric rings in Figure 2 indicate that the whole film is uniformly thick within the accuracy of the optical measurement, that is, within less than 1%. From experience we estimate that the film is uniformly thick down to the molecular layer level.

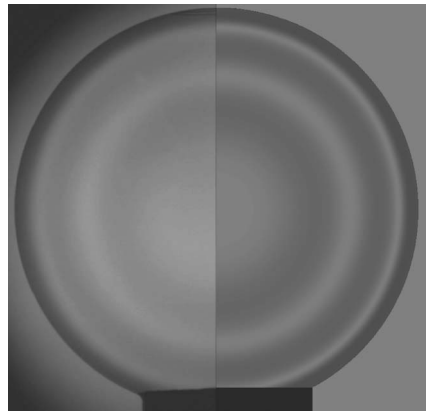

Figure 2. Simulation of the optical transmission of a smectic bubble in monochromatic light of 535 nm wavelength. The radius is 4.58 mm. A uniform thickness of 1.785 μm has been assumed. The experimental image on the left-hand side has been background corrected and contrast enhanced.

The images of the soap bubbles in monochromatic light are completely different. Owing to drainage and gravitation, a non-vanishing vertical film thickness gradient appears. As is seen from a qualitative comparison of the experimental and simulated images (Figures 3 and 4), the films are much thicker at the bottom than at the top. An unambiguous measurement of the film thickness is possible only where front and back sides have approximately the same thickness; this is condition is satisfied in the top part of the bubble in Figure 4(a). The calculated image assumes a continuous thickness gradient. In thick soap films, the absolute interference order of a given fringe is not always measurable unambiguously, it may vary by ± 1 order. Measurements with different monochromatic wavelengths are difficult since the film thickness is not in equilibrium. Thus, the optical measurements give a reliable thickness gradient and time evolution of the film thickness gradient and time evolution of the film thickness in the cause of the rupture process, but yield only an approximate absolute value.

3.2 Rim velocity

The inviscid film model assumes that the momentum generated by film rupture is entirely transferred to the motion of the rim that transports the excess material. The momentum balance, in combination with the

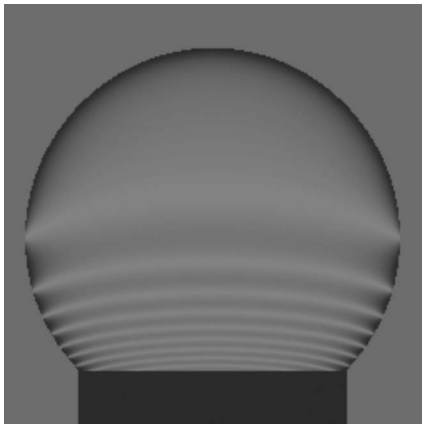

Figure 3. Simulation of the optical transmission of a soap bubble (same as in Figure 4 before rupture) in monochromatic light of 535 nm wavelength. In this image, an exponentially decreasing film thickness along the vertical, from 6.37 μm at the capillary to 135 nm at the bubble top, has been assumed. Further it is assumed that the film thickness is the same for all azimuthal positions at a given height. The simulation shows the characteristic upward bend of the interference bands (indicating the direction of the film thickness gradient) as can be seen in the experimental images. The number and positions of the bands give a rough measure of the film thickness profile.

assumption that the remaining film is at rest, leads to the differential equation for the momentum change of a rim segment with length ℓ:

$$2\sigma\ell = \frac{d}{dt}(m_{\mathrm{rim}} v)$$

where m_{rim} is the mass of the material in the rim per length ℓ of the border (for a straight edge moving on a plane film it is $m_{\mathrm{rim}} = \int_0^t \delta(x(t))\rho v\ell\, dt$), x is the momentary position of the rim and $\delta(x(t))$ is the film thickness immediately in front of the moving rim. In the case of a film of uniform thickness δ, the constant Culick velocity of (1) and $\dot{v} = 0$ solves this equation. The kinetic energy of each portion of liquid material moving in the rim remains constant. The surface energy of the material absorbed per unit time is transformed into kinetic energy of the same material with a constant efficiency of $\frac{1}{2}$. Thus, it is irrelevant for a uniform film whether the edge is straight or circular, or whether the film is planar or bent (*12*). The situation is different if the film thickness is inhomogeneous. We consider two cases here, a flat film with thickness gradient perpendicular to the propagation direction of the edge (vertical soap film with vertically propagating straight edge) and a bursting spherical bubble in the same geometry.

For simplicity, the quantity $v_0^2(t) = 2\sigma/(\rho\delta(x(t))$ is introduced, x is the momentary position of the edge. For a flat film, one finds

$$\dot{v}(t) = \left(1 - \frac{v^2(t)}{v_0^2(t)}\right) \Big/ \left(\int_0^t \frac{v(t)}{v_0^2(t)}\, dt\right) \qquad (2)$$

while for the spherical film and a horizontal circular edge, parallel to the lines of equal film thickness, moving downwards (bubble pierced on top, Figure 5), the velocity has to be determined from

$$\dot{v}(t) = \sin\theta(t)\left(1 - \frac{v^2(t)}{v_0^2(t)}\right) \Big/ \left(\int_0^t \frac{v(t)}{v_0^2(t)} \sin\theta(t)\, dt\right). \quad (3)$$

Here, $\theta(t)$ is the momentary polar angle of the edge.

In the rupture experiments with smectic films, where the film thickness is constant, the edges practically start with velocity v_0, an initial acceleration phase is not resolved. Figure 6(a) shows two typical measurements of the rim velocity for smectic bubbles of uniform thickness. The solid lines correspond to Culick's model. An acceleration phase can be observed only in bubbles where different regions of distinct film thicknesses are present (see, e.g., Figure 9 below). When the front hits the dislocation line, and enters a region of thicker film, an (negative) acceleration is observed and the velocity of the rim slows down quickly. This is evident in Figure 6(c) where the vertical dashed line

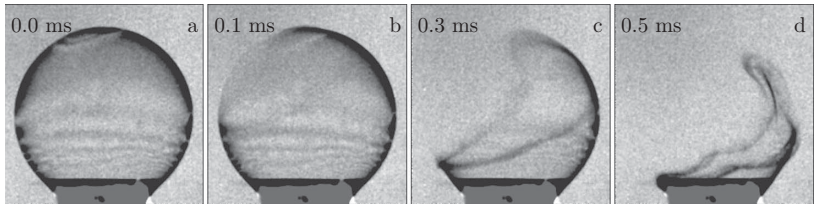

Figure 4. Time series of the rupture of a soap bubble. The characteristic interference patterns arise from the vertical film thickness gradient (cf. Figure 3). There is no detectable darkening during rupture. The radius of the bubble is 5.2 mm. The images are contrast enhanced and background corrected.

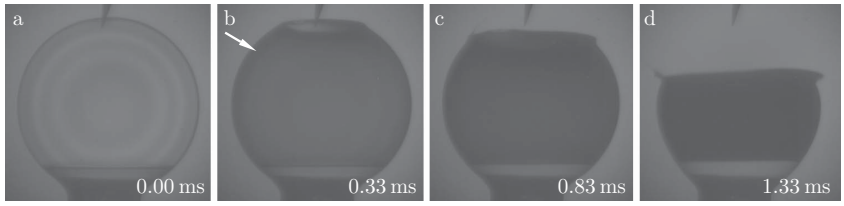

Figure 5. Time series of the rupture of a smectic A bubble. The film thickness is 2310 nm and the radius is 4.4. mm. There occurs a global darkening and, in addition, a black front propagates ahead of the rim (see the arrow in (b)). The images are contrast enhanced and background corrected.

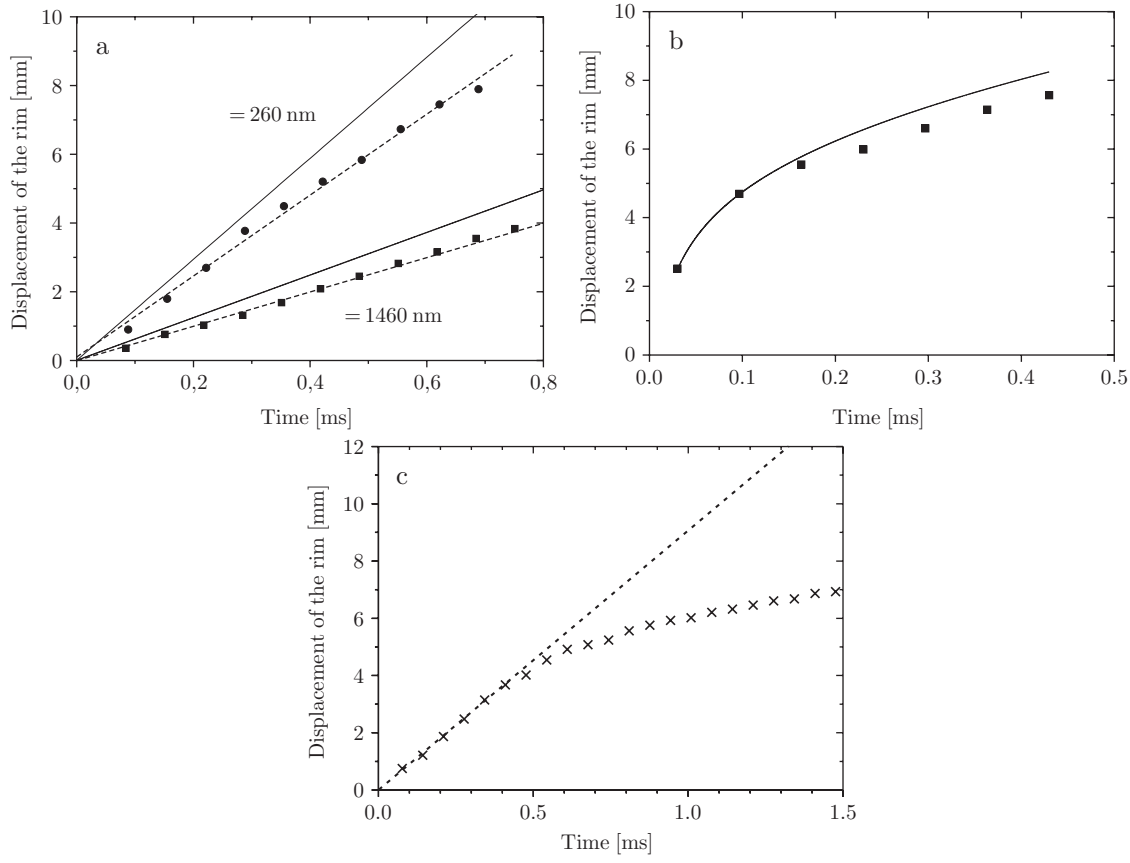

Figure 6. (a) Rupture dynamics of a smectic bubble with uniform film thickness of 1.46 μm, 4.5 mm radius (squares) and 260 nm, 5.1 mm radius (circles). The velocities of the rim are constant and initial acceleration phases are not resolvable. The solid lines represent Culick's model with the known parameters of 8CB. (b) Soap film with continuous film thickness gradient, see Figures 3 and 4. The solid line was calculated numerically from (3) with the optically determined thickness profile $\delta(\phi) = 0.625$ μm exp (1.1143(1 – cos ϕ) – 0.201 μm, ϕ is the polar angle of the hole. (c) Smectic bubble of 4.5 mm radius, with two regions of different film thicknesses (Figure 9(a)–(c)). The film in the upper hemisphere was 1.9 μm thick, while in the bottom part it was much thicker than 10 μm. The dashed line represents (1). The rim velocity slows down even before the rim hits the dislocation step, and a new asymptotic velocity corresponding to the changed film thickness is approached gradually.

marks the instant when the edge hits the dislocation step. Interestingly, the velocity already slows down before the edge has reached this step.

When the film thickness is inhomogeneous, (3) can be solved only numerically, provided some model or experimental data for the film profile $\delta(x)$ is available. In that case, the solutions depend not only on the film thickness profile but also on the hole geometry; the solutions differ for a straight edge on a planar film, for a circular edge in a planar film and for holes in

spherical bubbles, cf. (2) and (3). It can be seen immediately from the images in (*9*) that the upward and downward moving fronts of the hole are moving at different velocities. The upward edge, collecting thinner film, is notably faster. The authors have determined an average velocity in (*9*).

Figure 6 compares the rupture dynamics of (a) a smectic bubble of uniform thickness with (c) a bubble with two uniformly thick regions and (b) a soap bubble with exponentially increasing film thickness from top to bottom. The linear fits give (a) $v = 5.4$ m s^{-1} for the uniform bubble of $\delta = 1.46$ μm film thickness and $R = 4.5$ mm radius, (b) $v = 14.7$ m s^{-1} for the uniform bubble of $\delta = 0.26$ μm film thickness and $R = 5.1$ mm radius and (c) $v = 9$ m s^{-1} for the region with thickness of 0.69 μm. These values agree with the solid lines determined from (3) within an accuracy of 10%. The asymptotic velocity of $v = 1.9$ m s^{-1} in (c) would correspond to a film thickness of 15.1 μm according to Culick's model. However, for such thick films it is not possible to determine δ experimentally from the interference fringes with sufficient accuracy. The soap film (b), owing to its nonuniform thickness, shows a typical slowing down of the rim velocity as the hole progresses towards the thicker film regions at the bottom. The curve calculated with (3) is in qualitative agreement with the experimental data, but shows some systematic deviation to lower values as in the smectic films. The surface tensions used in the calculations are $\sigma = 0.028$ N m^{-1} (see (*31*)) for the smectic material and 0.0335 N m^{-1} for the soap film, determined with a Wilhelmy balance in an independent experiment.

3.3 Scattering of transmitted light

Figure 5 shows a typical burst experiment in smectic A recorded in monochromatic parallel light in transmission, and Figure 4 shows a similar experiment with a soap bubble. For smectic A bubbles, the transmitted light intensity decreases after the puncture (Figure 5). Initially, the interference fringes still remain visible in transmission (Figure 5(b)). Then, there is a very fast global darkening of the films (bottom of Figures 5(c) and (d)). It was impossible with our experimental technique to resolve a front velocity. The darkening intensifies continuously and homogeneously during rupture, independent of the film thickness in sufficiently thick films. However, films with thickness well below 500 nm burst in such short timescales that the darkening is not visible in the time series.

In addition to this global darkening, a black front spreads over thick films (micrometer film thickness) with a certain finite velocity. The global darkening and the dark front are hard to distinguish in the experiment; they are presumably of similar origin. The velocity of this front seems to be quite independent of the film thickness. Since the *rim* velocity depends on the film thickness δ, the black front can only be observed within a certain film thickness range. In thin films the rim is faster than the typical velocity of the black front. In the case of very thick films, the global darkening dominates the transmission characteristics and the black front is difficult to identify.

This darkening of the films in transmission during rupture has been identified as a consequence of light scattering (*12*). This is particularly evident from the images in Figure 7 which have been taken under indirect (dark field) illumination. After piercing of the bubble, the film starts to brighten up gradually, which provides evidence of some strong scattering (a faint image of the upper part of the initial bubble in these pictures is an artifact: an afterimage of the camera at high speed and low illumination intensity).

Since a similar scattering as in smectic bubbles has not been reported earlier in soap films, it was one of the aims of this study to analyse whether this is a consequence of different film structures or of the different observation techniques. Figures 4 and 8 provide evidence that this difference between the smectic and soap films cannot be attributed to the observation technique. The sequence in Figure 4 shows a typical soap bubble bursting. No darkening is observed in transmission, even though the film is several micrometres thick at the bottom, nor does one observe brightening at indirect illumination. This observation is independent of the initial film thickness profile. The details of soap film rupture can be seen in Figure 8.

The reason for the scattering could be a dynamic phenomenon, the peristaltic motion (see Figure 12) of the film or static inhomogeneities such as focal-conic domain formation. We interpret the intense scattering of the bursting smectic film with the assumption that transversal waves propagate on the film. These waves undulate the film surfaces in a wavelength range of micrometres. Such undulations can be classified, in principle, into two types.

Capillary waves where the two film surfaces are in phase represent the first type. Such an undulation leaves the local film thickness unchanged; it is thus not coupled to modulations of the smectic layer thickness. The propagation speed of such capillary waves, v_s, is given by $v_s = \sqrt{2\sigma/\rho\delta}$. A comparison with the velocity of the edge, (*1*), shows that the two velocities are equal. Consequently, capillary waves with in-phase undulations of the upper and lower film surfaces (bending mode (*19*)) do not travel faster than the rim, and consequently they do not penetrate the remaining film in front of the hole edge, irrespective of the film

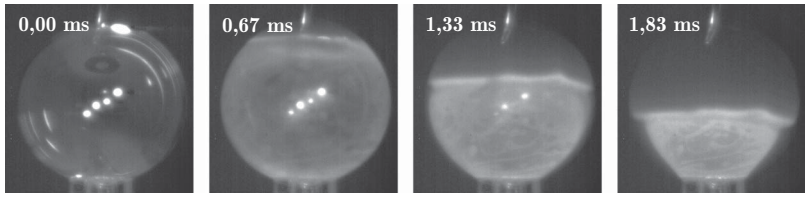

Figure 7. Bursting smectic bubble observed under indirect illumination. The light source illuminates the bubble at 90° to the observation direction. Initially, one can see the reflections of the light sources and some mirror images. After rupture, the smectic film brightens up globally due to light scattering.

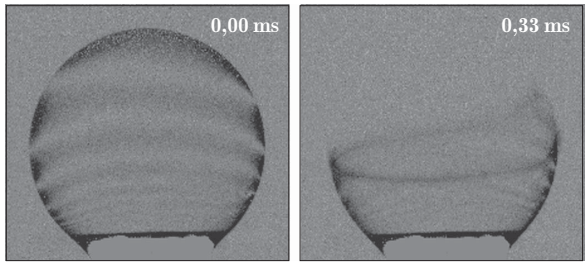

Figure 8. Image of a bursting soap bubble compared with that of the initial undistorted bubble (background subtracted and contrast enhanced). The bubble radius is 3.8 mm. Evidently, the transmission characteristics of the remaining film do not change during rupture and there is no increased light scattering.

thickness. This holds for soap films as well as for smectic A films.

Strictly, in smectic films an additional term related to the orientational elasticity enters the equation for the wave velocity. The energy per film area connected with this term is of the order of $Kq^2\delta$, with the wave number q and the splay elastic constant K. It is orders of magnitude smaller than the surface tension term 2σ. With typical values of $\sigma \approx 10^{-2}$ N m^{-1}, $K \approx 10^{-11}$ N, $q \approx 10^{-6}$ m^{-1}, $\delta = 10^{-6}$ m, one finds a ratio $2\sigma/(Kq^2\delta) > 10^3$. Thus, it is justified to neglect the orientational elastic terms for the capillary wave velocity.

Another aspect of these symmetric film surface undulations concerns their optical properties. Capillary waves which do not modulate the film thickness have insignificant effects on plane light waves penetrating the film, that is, their contribution to the scattering profile and scattering efficiency of the film is rather small. Even if such mechanical waves would precede the rim motion, they would hardly be observable optically in transmission.

We also exclude the static interpretation of the scattering phenomenon, since such a formation of focal-conic domains in the films would either occur instantaneously, that is, with the speed of sound in the film, or as a consequence of the peristaltic waves. In the latter case, such layer undulations would be a secondary effect.

The second type of film undulations, waves that involve antisymmetric fluctuations of the two film surfaces (peristaltic waves, squeezing modes (*19*)) differ essentially in soap films and smectic films, because of the smectic layer compression elasticity. Since such waves modulate the local film thickness, they not only cause strong scattering of transmitted light (*20*), but they also couple to the smectic layer compression constant B, a material parameter of the order of several megapascals, which describes the elasticity of smectic molecular layers with respect to compression and dilatation. A back of the envelope calculation of the layer compression elasticity term shows that peristaltic undulations move with a velocity of the order of $\sqrt{B/\rho}$ (see (*21, 23*)) instead of the value $\sqrt{2\sigma/(\delta\rho)}$ in a non-layered system (*22*). This velocity is two orders of magnitude larger than the latter case, at least in films in the micrometre thickness range. This leads to a faster propagation of peristaltic waves in the smectic films, their velocity is of the order of 30 to 100 m s^{-1}. When such waves are emitted near the hole edge, they can precede the rim during rupture and lead to the characteristic darkening of the transmission images. As has been determined in earlier experiments (*12*), the typical wavelengths of these peristaltic undulations are of the order of a few micrometres. A quantitative analysis of the propagation of all of these types of mechanical waves in smectic films may be possible on the basis of theoretical models, developed for example by Holyst (*24*), Fedorov *et al.* (*25*) and Chen and Jasnov (*26*), but such a treatment is beyond the scope of this experimental study. When the layer compression term dominates, their propagation velocity is $v_p \approx \sqrt{B/\rho}$. This consideration explains why common soap films, which lack the smectic layer compressibility term, do not show the pronounced scattering during rupture.

From an optics point of view, peristaltic waves modify locally the optical path of transmitted light, unlike the capillary waves described above. The optical path difference created by a few per cent film

thickness modulation in a micrometrethick film is sufficient to make the film turbid in transmission, and brighten the film under indirect illumination (Figure 7).

Two effects may be responsible for the fact that thin smectic films do not show the pronounced scattering. First, the velocity of peristaltic waves is independent of film thickness if the layer compression effect dominates, while the rim velocity is proportional to $1/\sqrt{\delta}$, so that in thin films the rim moves faster than the peristaltic waves. Second, the film undulations and the optical scattering efficiency both decrease with decreasing film thickness, so that thin films may appear nearly transparent even if low-amplitude peristaltic undulations are present.

Interestingly, the peristaltic waves are reflected at large thickness steps in the film, as is seen in Figure 9(b) and (c). Only after the edge has passed the dislocations of the smectic layers does the bottom half of the bubble darken.

3.4 Film thickening during rupture

Since the dynamic model assumes that the film material stays at rest until it is collected in the moving rim, the original film thickness in an inviscid bubble should not be influenced by rupture before the arrival of the film edge. Our optical transmission measurements with monochromatic light allow a test of this hypothesis for smectic and soap bubbles. A shift of the fringe positions is taken as a measure of local changes in film thickness. In soap films, the fringes can be monitored during the complete rupture process, while in smectic films, it is possible to discriminate between the fringe positions only until the onset of the strong light scattering. Nevertheless, both types of films reveal a thickness increment during rupture. The thickening dynamics of the soap films differs remarkably from that of smectic A films.

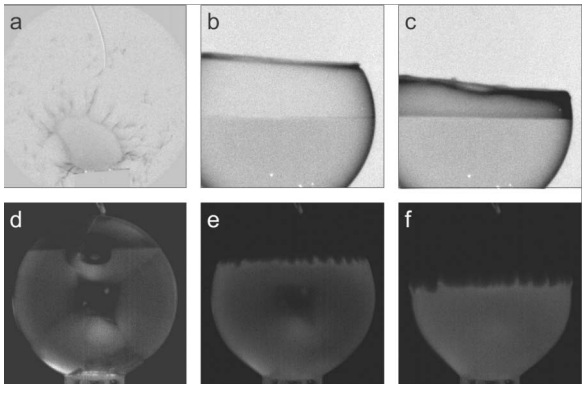

Figure 9. (a) Fragmentation and filamentation of the film edge in a thin film (close to the end of the rupture process), bubble radius R = 3.3 mm, film thickness δ = 135 nm; and (b), (c) straight progressing rim in a thick film, R = 3.2 mm, δ = 445 nm, with images taken 1.17 ms and 1.67 ms after rupture, respectively. (d)–(f) Bubble with inhomogeneous thickness (d) before rupture, (e) 0.4 ms and (f) 0.53 ms after rupture, R = 3.6 mm, δ = 1950 nm in the lower part, only a few nanometers in the top part. The undulation instability of the rim sets in after the front has hit the layer thickness step and is slowed down subsequently. The images in (d)–(f) have been obtained with the dark field diffuse illumination technique. Artifacts seen on the bubble (d) reflect the dark screen behind the bubble. They disappear when the film becomes strongly scattering during rupture (e), (f).

A global thickening takes place in smectic A films at the very early stage of the rupture. The shift of the fringes in the equatorial plane, as shown in Figure 10(a), is representative of a global uniform film thickness change. The figure shows the time evolution of a horizontal cross section near the equator of a smectic A bubble with initial film thickness δ = 2.31 μm. The white arrow in Figure 10(a) marks the position of one of the intensity maxima. The bright ring of constructive interference is displaced outwards. Even though it is difficult to measure the film thickness change quantitatively during the onset of scattering, the increment of the film thickness is clearly uniform (the fringes remain concentric rings). The graph to the right-hand side of Figure 10(a) indicates the relative thickness at various stages of the rupture, the film thickness increment $\Delta\delta$: δ was of the order of 1.5%. This order of magnitude has been found to be quite independent of the initial film thickness in several experiments with films of thicknesses in the micrometre range. Since the displacement of the interference fringes can only be observed until the transmission pattern is superimposed by scattering, we cannot definitely state what asymptotic value is finally reached in the smectic films. Figure 10(b) gives the observed film thickness increments for a series of bubbles. A trend to larger thickness changes with higher film thickness is clearly observable; apparently the relative thickness change (before the onset of scattering) is of the same order in all films.

In soap films, a similar thickening was measurable. The initial exponential increase of the vertical film thickness profile results in a characteristic pattern as can be seen in Figures 3 and 4. During rupture, the interference maxima are displaced upwards, which reflects a thickening of the film.

Figure 11 shows the analysis of two thickness profiles at $t = t_0$ and t_0 + 0.17 ms. The dots refer to the observed interference maxima. In the soap films, because of the absence of the strong scattering, the film thickness change can be monitored until the rim collects the respective film area. In the second profile of the figure, 0.17 ms after the rupture had started, the

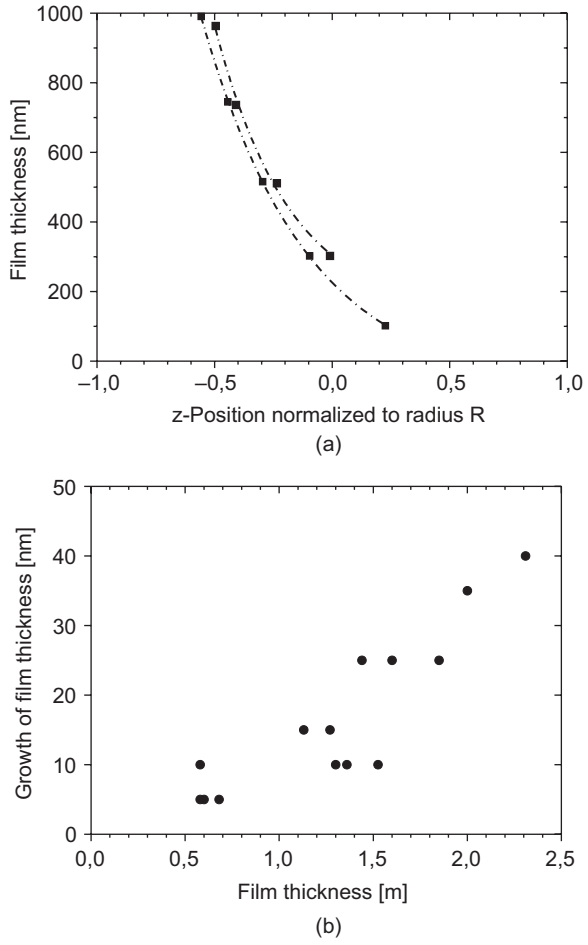

Figure 10. (a) Time evolution of the horizontal cross section of a smectic bubble with initial film thickness $\delta = 2.31\ \mu$m. The time axis runs from top to bottom. The stack consists of nine images and puncture occurs at $t = 0$. Contrast has been enhanced. During rupture, the interference maximum shifts outward (arrow), indicating a global thickening of the film. The graph at the right-hand side visualizes the approximate film thickness change for each image. (b) Film thickness dependence of the detectable thickness change before scattering covers the transmission pattern.

rim has already passed the interference maximum of the first-order fringe. The film thickness increase in this region was approximately (15 ± 5)%. The excess material that leads to an increasing local film thickness stems from the opening edge of the film hole. This has been verified from the observation of small tracer (dust) particles which move in the same direction as the edge.

3.5 *Rim fragmentation*

During the rupture of inviscid soap films, a typical fragmentation of the progressing edge into small droplets has been reported earlier (*9*), and the same

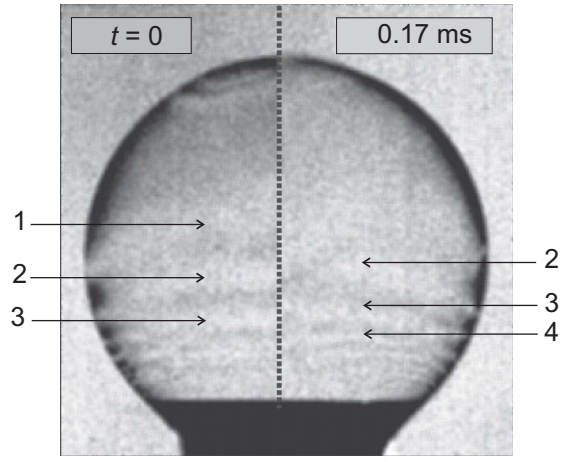

Figure 11. The left half sphere shows a bubble at time t_0, the right half presents the same bubble at the time $t_0 + 0.17$ ms, the dashed line separates the two half-images. The images are background corrected and contrast enhanced. All interference maxima in the right-hand picture are shifted up with respect to the corresponding maxima in the right-hand image (the top first-order maximum is already caught up by the rim at the top). The upward shift of these fringes corresponds to a gradual thickening.

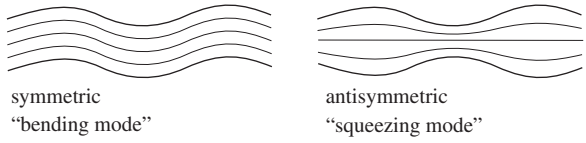

Figure 12. Sketch of symmetric (bending) and antisymmetric (squeezing) modes of film surface fluctuations of smectic free standing films.

phenomenon occurs in thin smectic films (*12*). The physical background for this instability is not yet fully understood. However, it is evident that this type of decomposition of the film edge is dependent on film thickness in smectic bubbles. This is demonstrated in Figure 9, which shows bursting smectic A films of different thickness: (a) is a bubble with uniform thickness, in (b), (c) the bubble has two regions of uniform thickness, and (d)–(f) show a bubble with a single, particularly large thickness step. In the thin film (a), the rim becomes unstable with respect to undulations, their lengths are of the order of a few hundred micrometres. The instability leads to the formation of irregular rim shapes and to a more or less pronounced fragmentation and droplet formation. In the thicker film (b), (c), the rim remains straight and compact until it collides with the film thickness step. Since the velocities of the bursts in the two films in Figure 9(a)–(c) differ only by roughly a factor of two and not by orders of magnitude, it is unlikely that this is an effect of different rim progression speeds. This is

discussed in a little more detail below. Smectic films with very inhomogeneous thickness represent an exception, as seen in Figure 9(d)–(f). When the front hits the layer thickness step, its velocity reduces almost instantly (here by almost one order of magnitude), and the edge starts to undulate. The initial thickness step is seen as a horizontal edge in the upper part of Figure 9(d).

4. Discussion and summary

The rupture of smectic and soap films follows essentially the same dynamics. The similarities between the experimental observations in the two materials manifest themselves primarily in the geometrical features of the collapse. In both types of materials, one observes the recession of the film material in a rim that moves with a velocity given by geometrical and material parameters. This feature is a direct consequence of the release of surface energy, its transformation into kinetic energy of the rim and partial dissipation. Even though the viscosities of the smectic material is higher than that of water by at least one order of magnitude, the principal feature of an inertial burst (constant rupture velocity) is maintained. In homogeneous smectic films, this is confirmed by time-resolved measurements of the rim position in uniformly thick films. In soap films, a direct confirmation of Culick's model is difficult because of the non-uniform film thickness. However, a numerical calculation of the momentary rim dynamics yields satisfactory qualitative agreement with the experimental observations.

An instability of the moving rim that leads to its decomposition and the scattering of small liquid droplets is observed both in soap films and very thin smectic films (*9, 12*). In thick smectic films (above several hundred nanometers film thickness) the rim remains straight and compact (*12*). Actually, such a formation of small droplets has been suggested by de Gennes (*27*) in an introductory lecture on the mechanics of soft interfaces. He proposed that the constant impact of the moving rim material onto the resting film could lead to a fragmentation of the film and a transfer of kinetic energy onto the emerging small droplets. The first part of this view seems to be confirmed by our experiments, at least in sufficiently thin films. Furthermore, according to de Gennes, the scattering of droplets could serve as a possible process to account for the above-mentioned discrepancy in the energy balance. Droplets escaping the rim in directions normal to the film, with a velocity comparable to the rim motion, would not change the momentum balance of (1) but save the energy balance without the necessity to introduce dissipative terms. They would slow down the rim motion. On the basis of our observations, we conclude that this interpretation does not hold for the investigated systems. The rim velocity is slightly below Culick's prediction in thin smectic films (with fragmenting edge) as well as in thick films (with compact edge), thus the fragmentation should not be responsible for the kinetic energy loss.

It is well known that fragmentation of thin liquid sheets can occur when the liquid object is moving rapidly in a surrounding medium (see (*28*) and references therein). Hanson *et al.* (*29*) have measured critical Weber numbers $We = \rho_{\mathrm{air}} u^2 r/\sigma$ for droplet fragmentation, with u being the difference of the velocities in the stagnation points and in the region of maximum flow (which is approximately equal to the rim velocity of (1) in our system), ρ_{air} being the air density, and r being the radius of the liquid object and σ being the surface tension. For different fluids, they found critical We above 1. On first glance, the edge geometry in this experiment looks similar to the bubble burst. In our system, the Weber number is two or three orders of magnitude below that value. One has to conclude that the mechanisms leading to fragmentation in Hanson *et al.*'s experiments is different from that in the bursting smectic and soap bubbles. Actually, the geometry differs in the direction of the film edge with respect to the bulk. In (*29*) the shock wave pulls the liquid from the bulk droplet, carrying the droplets with the external fluid. In the bursting bubble geometry, the rim hits the resting film and permanently creates collisions, which may lead to the instability of the edge and fragmentation in the bubble experiments.

Both smectic and soap bubbles show a thickening of the film in front of the rim and this involves practically the complete bubble remainder. This has not been observed in soap bubbles before, presumably because the experiments (*9*) have been performed in white light where the film thickness has not been monitored during rupture. Drainage cannot be responsible in our bubbles, even though the gradient of the gravitational potential is parallel to the rim motion. This process is much slower than the film thickness changes observed during rupture.

On the other hand, it should be mentioned here that in planar films with thickness gradients, a complex thickness change can precede the advent of the rim (*30*). The experiments by Liang *et al.* (*30*), performed in monochromatic light, show a much more intricate scenario than that observed in our bubbles. The characteristics of upward moving fronts differ qualitatively from those of downward moving fronts in vertically suspended films. Both thickening and subsequent thinning are observed in the downward front or, in other words, in the front that moves in

the direction of positive film thickness gradient. The front moving against the initial film thickness gradient is preceded by a continuous thickening of the film. The concentration and type of surfactant play an essential role in these systems, but the authors have no conclusive explanation of this unusual behaviour. Definitely, the thickening in the smectic films is essentially different from that observed by Liang *et al*. The thickness change occurs (within the time resolution of our experiment) uniformly in the whole bubble, and not in the form of a front or aureole.

Continuous thickening during rupture is a characteristic feature of viscous bubbles, where it has been measured quantitatively (*13, 14*), as stated in the introduction. The effect observed in the inviscid soap and smectic bubbles is clearly observable and quantitatively measurable, but is much weaker, and certainly of different origin. A possible explanation of the thickening of bursting smectic films is the increased pressure in the film after rupture. The inner pressure of a smectic film before rupture is slightly below the external air pressure (because of the Laplace pressure of the meniscus (*32–34*)). After rupture, the curvature at the edge of the order of a few micrometres creates a large Laplace pressure in the film. This inner excess pressure may be responsible for a sudden viscoelastic response of the layers, connected with a contraction in the film plane and dilation normal to the layers. In the smectic films, we find that the thickening of a uniform film during rupture amounts to a relative thickness change Δ/δ of a few per cent. A rough estimate gives pressures of the order of $B\Delta/\delta \approx 150$ kPa, which corresponds to the Laplace pressure of a film edge with a diameter of about 200 nm. This is a realistic value for the thin films shown in Figure 10(b), but our interpretation cannot explain why the *relative* film thickness increment is almost the same for all films, that is, unexpectedly large in the thicker films.

In the soap films, where the quantitative measurement is difficult because of the spatial inhomogeneity of the films, the thickening is much more pronounced and it reaches far more than 10 per cent of the initial film thickness. Again, the difference can be attributed to the smectic layer compression modulus B which counteracts a change of the smectic layer spacing.

Finally, the smectic films (except very thin films) are characterized by a pronounced diffuse light scattering after rupture. This leads to a darkening of the transmission images, and on the other hand to a brightening when the films are indirectly illuminated. The reason for this scattering is a local modulation of the optical path of transmitted light, which could either be caused by undulations of the layers connected to a modulation of the effective refractive index, or caused by a modulated film thickness. The arguments in favour of the latter interpretation are the large scattering intensity even in films below micrometre thickness, and the correct estimate of the propagation velocity of peristaltic waves in a smectic film (*23*). In common smectics, this velocity is faster than the propagation speed of the rim of the bursting film and it depends on the layer elasticity B. If the film has no inner layer structure ($B = 0$), such waves do not occur. Therefore, the phenomenon is absent in the soap film experiments. The numerical analysis of these waves will be published elsewhere. Another argument that supports the peristaltic wave model is derived from the observation of the darkening effect in films with large thickness steps (Figure 9(c)). We find that the film beyond the thickness step darkens only after the rim has passed this step into the thicker region. This can be explained by a reflection (or absorption) of the mechanical waves at the thickness step. There is no obvious reason why ordinary sound, that is, density and pressure pulses, should not pass such layer steps. They do not depend on the film thickness. On the other hand, the propagation of peristaltic undulations is film thickness dependent, as the mathematical treatment shows (*23*). At the border of a much thicker film region, such waves may be reflected almost completely, as is seen in Figure 9(c).

Acknowledgements

The authors would like to thank Ulrike Kornek for her collaboration in some of the experiments and Christian Bohley for assistance in FEM calculations of light propagation through undulated films. We acknowledge financial support by the Deutsche Forschungsgemeinschaft under Grant STA 452/20.

References

(1) Dupré, A. *Théorie Mécanique de la Chaleur*; Gauthiers-Villars: Paris, 1869.
(2) Dupré, A. *Ann. Chim. Phys*. **1867**, *11*, 3018.
(3) Lord Rayleigh (Strutt, W.) *Sci. Papers* **1902**, *3*, 441–451.
(4) Culick, F. E. C. *J. Appl. Phys*. **1960**, *31*, 1128–1129.
(5) Taylor, G.I. *Proc. R. Soc. Lond. A* **1959**, *253*, 313–321.
(6) McEntee, W.R.; Mysels, K.J. *J. Phys. Chem*. **1969**, *73*, 3018–3028.
(7) Frankel, S.; Mysels, K.J. *J. Phys. Chem*. **1969**, *73*, 3028–3038.
(8) Ranz, W.E. *J. Appl. Phys*. **1959**, *30*, 1950.
(9) Pandit, A.B.; Davidson, J.F. *J. Fluid Mech*. **1990**, *212*, 11–24.
(10) Evers, J.; Shulepov, S.Y.; Frens, G. *Phys. Rev. Lett*. **1997**, *79*, 4850.
(11) Evers, J.; Nijman, E.J.; Frens, G. *Coll. Surf. A* **1999**, *149*, 521–527.
(12) Müller, F.; Kornek, U.; Stannarius, R. *Phys. Rev. E* **2007**, *75*, 065302.

(13) Debrégeas, G.; Martin, P.; Brochard-Wyard, F. *Phys. Rev. Lett*. **1995**, *75*, 3885–3889.
(14) Debrégeas, G.; de Gennes, P.G.; Brochard-Wyard, F. *Science* **1998**, *279*, 1704–1707.
(15) Schneider, F. *Phys. Rev. E* **2006**, *74*, 021709.
(16) Thoroddsen, S.T.; Etoh, T.G.; Takehara, K. *Annu. Rev. Fluid Mech*. **2008**, *40*, 257–285.
(17) Stannarius, R.; Cramer, C.; Schüring, H. *Mol. Cryst. Liq. Cryst*. **2000**, *350*, 297–305
(18) Dunmur, D.A.; Manterfield, M.R.; Miller, W.H.; Dunleavy, J.K. *Mol. Cryst. Liq. Cryst*. **1978**, *45*, 127.
(19) Sonin, A.A. *Freely Suspended Liquid Crystalline Films*; Wiley: New York, 1998.
(20) 20. Müller, F.; Bohley, Ch. Numerical calculation of light propagation with COMSOL package, unpublished.
(21) de Gennes, P.G.; Prost, J. *The Physics of Liquid Crystals*; Clarendon Press: Oxford, 1993.
(22) Taylor, G.I. *Proc. R. Soc. London A* **1959**, *253*, 296.
(23) 23. Müller, F.; Bohley, Ch.; Stannarius, R. unpublished.
(24) Hołyst, R. *Phys. Rev. A* **1992**, *46*, 6748–6749.
(25) Fedorov, D.O.; Romanov, V.P.; Ulyanov, S.V. *Phys. Rev. E* **2000**, *62*, 681–688
(26) Chen, H.-Y.; Jasnov, D. *Phys. Rev. E* **1998**, *57*, 5639–5643.
(27) de Gennes, P.G. *Faraday Discuss*. **1996**, *104*, 1–8.
(28) Villermaux, E. *Annu. Rev. Fluid Mech*. **2007**, *39*, 419–446.
(29) Hanson, A.R.; Domich, E.G.; Adams, H.S. *Phys. Fluids* **1963**, *6*, 1070–1080.
(30) Liang, N.Y.; Chan, C.K.; Choi, H.J. *Phys. Rev. E* **1996**, *54*, R3117.
(31) Stannarius, R.; Cramer, C. *Liq. Cryst*. **1997**, *23*, 371.
(32) Picano, F.; Oswald, P.; Kats, E. *Phys. Rev. E* **2001**, *63*, 021705.
(33) Jaquet, R.; Schneider, F. *Phys. Rev. E* **2003**, *67*, 021707.
(34) Jaquet, R.; Schneider, F. *Phys. Rev. E* **2003**, *68*, 039902(E).